

## LETTERS MARS

# **Aeolian processes at the Mars Exploration Rover Meridiani Planum landing site**

R. Sullivan<sup>1</sup>, D. Banfield<sup>1</sup>, J. F. Bell III<sup>1</sup>, W. Calvin<sup>2</sup>, D. Fike<sup>3</sup>, M. Golombek<sup>4</sup>, R. Greeley<sup>5</sup>, J. Grotzinger<sup>3</sup>, K. Herkenhoff<sup>6</sup>, D. Jerolmack<sup>3</sup>, M. Malin<sup>7</sup>, D. Ming<sup>8</sup>, L. A. Soderblom<sup>6</sup>, S. W. Squyres<sup>1</sup>, S. Thompson<sup>5</sup>, W. A. Watters<sup>3</sup>, C. M. Weitz<sup>9</sup> & A. Yen<sup>4</sup>

The martian surface is a natural laboratory for testing our understanding of the physics of aeolian (wind-related) processes in an environment different from that of Earth. Martian surface markings and atmospheric opacity are time-variable, indicating that fine particles at the surface are mobilized regularly by wind<sup>1–3</sup>. Regolith (unconsolidated surface material) at the Mars Exploration Rover Opportunity's landing site has been affected greatly by wind, which has created and reoriented bedforms, sorted grains, and eroded bedrock. Aeolian features here preserve a unique record of changing wind direction and wind strength. Here we present an *in situ* examination of a martian bright wind streak, which provides evidence consistent with a previously proposed formational model<sup>4,5</sup> for such features. We also show that a widely used criterion for distinguishing between aeolian saltation- and suspension-dominated grain behaviour is different on Mars, and that estimated wind friction speeds between 2 and 3 m s<sup>-1</sup>, most recently from the northwest, are associated with recent global dust storms, providing ground truth for climate model predictions.

Pre-landing orbiter observations of Opportunity's landing site showed bright and dark streaks tapering away from craters on the Meridiani plains. From observations of similar features distributed across many locations on Mars, streak orientations indicate

formative wind directions<sup>6–8</sup>. High-resolution images within the 117 km × 18 km landing ellipse obtained over several years show bright streak directions that indicate winds from the northwest and southeast<sup>9</sup>. What has not been recognized previously, however, is that this apparent bimodality of wind direction has a significant time dependence. Images obtained before the major 2001 dust storm are more likely to show bright streaks oriented in the opposite direction from images obtained after the storm waned. Rare overlapping image pairs provide two examples of an individual streak changing orientation after the intervening 2001 dust storm (Fig. 1). On this basis, we conclude that bright wind streak materials encountered by Opportunity are transient deposits mobilized by strong winds associated with major dust storms. Opportunity performed the first *in situ* investigation of a martian wind streak, evaluating the origin of Eagle crater's bright wind streak against predictive models<sup>4,5,10</sup>. Opportunity focused on a bright patch of material just outside the southeast rim of Eagle crater. Pancam visible/near-infrared spectra of this material are similar to global air fall dust measured telescopically<sup>11</sup>. Miniature Thermal Emission Spectrometer data of the same material can be modelled with ~70% air fall dust. Alpha Particle X-ray Spectrometer (APXS) and Mössbauer data also permit an air fall dust interpretation<sup>12–14</sup>. The APXS results

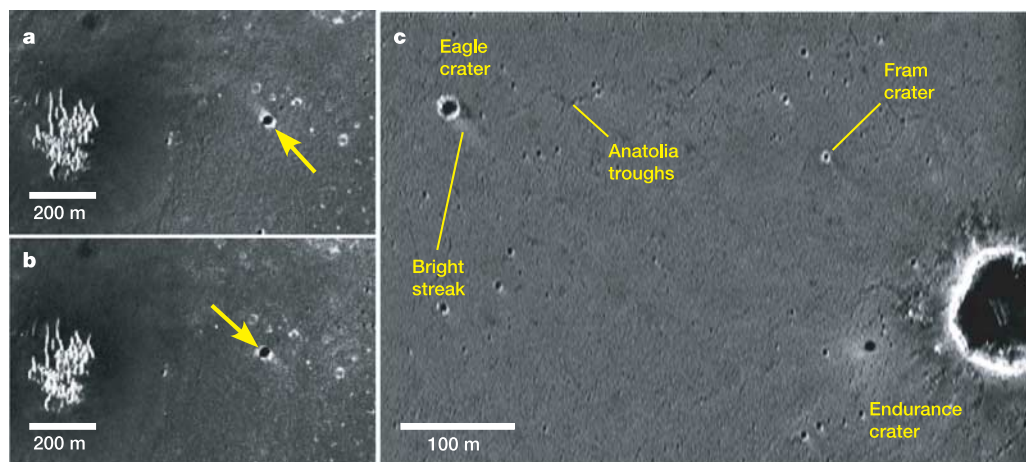


**Figure 1 | Bright wind streaks on Meridiani Planum.** **a, b**, Mars Global Surveyor Mars Orbiter Camera (MOC) views of a reversing bright wind streak at 5.3°W, 2.0°S. A global dust storm affected the planet during the

16-month interval between MOC images E0200373 (top) and E1800855 (bottom). **c**, Mars Exploration Rover descent camera image of the landing site, showing landmarks referred to in the text.

<sup>1</sup>Department of Astronomy/CRSR, Cornell University, Ithaca, New York 14853, USA. <sup>2</sup>Geological Sciences, University of Nevada, Reno, Nevada 89557, USA. <sup>3</sup>Earth, Atmospheric, and Planetary Sciences, Massachusetts Institute of Technology, Cambridge, Massachusetts 02139, USA. <sup>4</sup>Jet Propulsion Laboratory, Pasadena, California 90119, USA. <sup>5</sup>Department of Geological Sciences, Arizona State University, Tempe, Arizona 85287-1404, USA. <sup>6</sup>US Geological Survey, Flagstaff, Arizona 86001, USA. <sup>7</sup>Malin Space Science Systems, San Diego, California 92191, USA. <sup>8</sup>NASA Johnson Space Center, Houston, Texas 77058, USA. <sup>9</sup>Planetary Science Institute, Tucson, Arizona 85719, USA.

show the bright material is not derived from the light-toned, sulphate-enriched outcrop within the crater. The streak itself derives its brightness from small bright deposits in areas associated with local surface roughness. We conclude that air fall dust, deposited in the partial wind shadow of Eagle crater, is responsible for the bright streak seen from orbit. These findings are consistent with a model proposed using relatively low-resolution Viking Orbiter data that predicted that patchy, discontinuous deposits of air fall dust would be distributed behind obstacles during periods of atmospheric thermal stability, for example, during major dust storms<sup>4,5</sup>.

The wind friction speed  $u_*$  is  $(\tau/\rho)^{1/2}$ , where  $\tau$  is shear stress applied to the surface and  $\rho$  is atmospheric density.  $u_{*t}$  is the threshold value of  $u_*$  required to initiate movement of a bed of particles, and is a function of gravity, and atmospheric and particle characteristics. The gradual transition from aeolian saltation to suspension is commonly defined where wind friction speed,  $u_*$ , for a particle begins to exceed its terminal fall velocity,  $u_F$  (refs 15–18). For terrestrial conditions this particle size is around 50  $\mu\text{m}$ , but is expected to be around 200  $\mu\text{m}$  for Mars owing to higher  $u_{*t}$  values for all particle sizes and lower gravity<sup>16,17</sup>. On Earth, dune sand is several times the transitional particle size, so this is anticipated also to be the case on Mars<sup>19</sup>. However, ripples on the floor of Eagle crater are

composed of basaltic grains 50–125  $\mu\text{m}$  in size. The  $u_F/u_{*t}$  ratio for these grains is only  $\sim 0.5$ . Therefore, the relationship between the  $u_F/u_{*t}$  ratio and particle behaviour must be different for Mars.

Under terrestrial conditions, ripples of silt grains can form with  $u_F/u_{*t} < 1$ , but these bedforms are in general confined to wind tunnels, under conditions of  $u_*$  only slightly exceeding  $u_{*t}$ , so that mobilized particles remain concentrated closely above the bed and particle trajectories are still relatively short<sup>20</sup>. It seems unlikely that these specific conditions, scaled appropriately for Mars, are indicated by the Eagle floor ripples composed of 50–125- $\mu\text{m}$  grains and other deposits in temporary aeolian traps seen along Opportunity's traverse. Another, less-restrictive explanation might involve the potential inadequacy of  $u_F/u_{*t}$  to characterize particle responsiveness to turbulence. A particle small enough to be lofted into suspension must be more responsive to the accelerations of turbulent eddies than to gravity. Therefore particle response time to achieve  $u_F$  might be significant. The lower martian atmospheric density (by a factor of 80) and  $\sim 25\%$  lower atmospheric dynamic viscosity should lengthen the particle response time to accelerations of turbulent eddies, requiring increased turbulent energy from higher wind speeds to achieve the same probability of suspension as on Earth. In this scenario, the transition from saltation to suspension on Mars

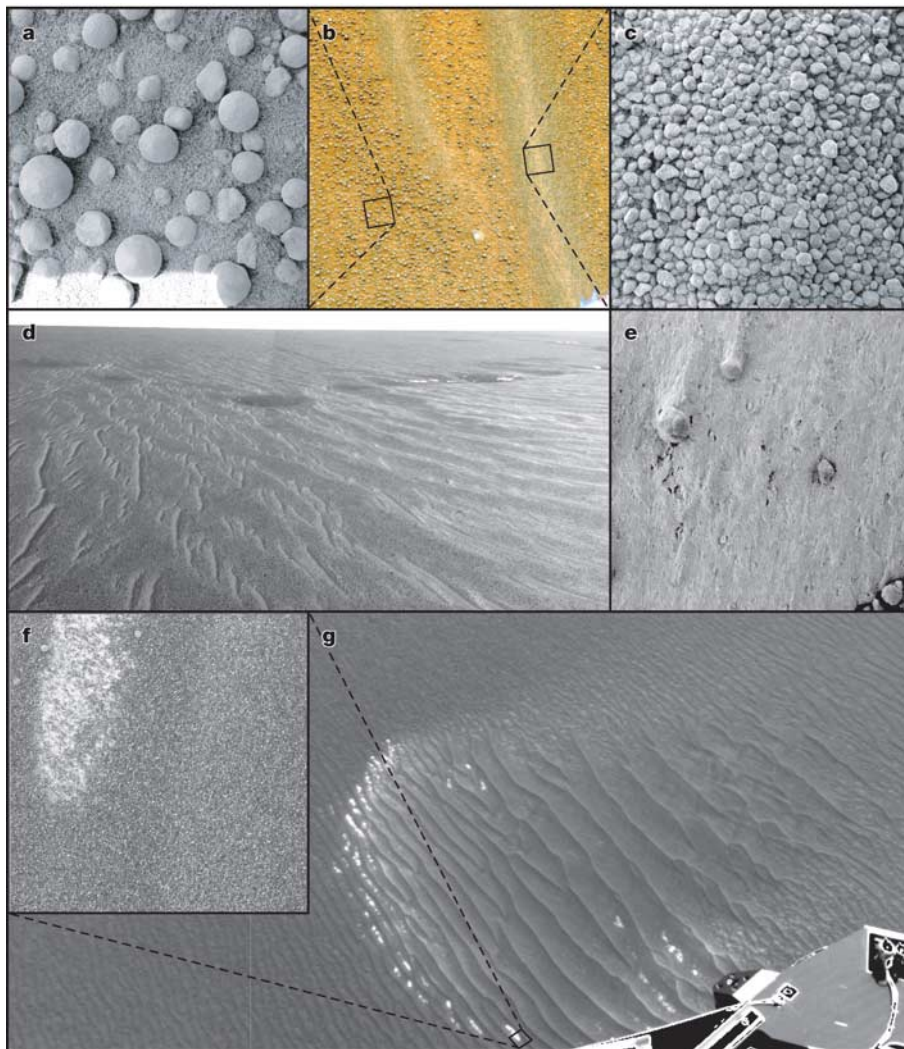


**Figure 2 | Bedforms and ventifacts at Meridiani Planum.** Microscopic Imager views are  $\sim 31$  mm across. **a–c**, False-colour Pancam (753 nm, 535 nm, 440 nm) view showing locations of Microscopic Imager close-ups of a ripple crest and an area between ripples. **d**, Navcam mosaic spanning  $80^\circ$  showing plains ripples organized into primary and secondary orientations.

**e**, Ventifacts on sulphate-enriched outcrop at Fram crater. **f**, Microscopic Imager view of basaltic sand ripples on Eagle crater floor. **g**, Navcam view of the same basaltic sand ripples. The longest wavelengths are  $\sim 11$  cm. Brighter material in some ripple troughs has been distributed to the right, downwind to the southeast.

is delayed to greater turbulent energies and smaller particle sizes than the  $u_F/u_{*t}$  ratio would suggest. Some support for this concept is provided by numerical simulations of martian saltation particle trajectories that predict that sand grains on Mars should achieve smaller fractions of entraining wind speed along their saltation trajectories than on Earth<sup>21</sup>.

Bedforms across the site can be organized into two groups based on correlated differences in constituents, morphology, and local setting: (1) plains ripples armoured with coarse sand; and (2) patches of ripples composed of 50–125- $\mu\text{m}$  basaltic sand that occur in local depressions. The wind direction indicated for basaltic sand ripples is aligned with the current bright streak direction where these features occur together, but is not aligned with winds indicated for the more extensive plains ripples. On the basis of these differences and the different wind speeds required to mobilize each bedform type, we develop a brief, recent aeolian history of the site that constrains estimates of local, near-surface wind speed and direction during recent major dust storms.

Ripples composed almost entirely of basaltic 50–125- $\mu\text{m}$  sand are found within craters, smaller pits, and structural troughs that apparently serve as particle traps (Fig. 2). Ripple profiles have smooth, continuously concave troughs connected by narrow crests (different from plains ripples). These sand ripples were examined on the floor of Eagle crater and on drifts among the Eagle crater outcrops, and were observed more distantly within the Anatolia trough system, the 9-m-diameter crater Fram, and within Endurance crater. The Eagle floor ripples occur in several distinct patches with different characteristic wavelengths. Orientations are about N38°E, and bright material deposited within some ripple troughs appears to have been partially redistributed approximately southeast along the crater floor, consistent with the most recent winds forming the much-larger exterior bright wind streak that extends S45°E from the crater. The Eagle crater floor ripples were trenched more easily by the rover wheel than any other material<sup>22</sup>, and open pore space between sand grains in these ripples is apparent in Microscopic Imager views. These bedforms are probably currently mobilized by the same recent winds that formed the bright wind streaks associated with Eagle crater and other craters in the area.

Plains ripples (Fig. 2) are covered with a monolayer of rounded, 1–2-mm fragments of haematite-enriched concretions, and have poorly sorted interiors dominated by a matrix of fine to very fine sand. Feature heights and widths are typically  $\sim 1$  cm and 10 cm, respectively, and crest-line lengths range up to 2 m. Larger examples occur on rims adjacent to shallow depressions. Areas between these ripples are dominated by 50–125- $\mu\text{m}$  basaltic grains that partly bury additional concretion fragments. Intact, spherical concretions several millimetres across are found scattered only between ripples<sup>23</sup>. Mössbauer contact plate impressions into areas between plains ripples reveal weak cohesion between basaltic grains. Unlike the loose basaltic sand grains observed within Eagle and Endurance craters, much of the 50–125- $\mu\text{m}$  sand out on the plains has evidently remained inactive long enough for cohesion to form between grains by some unknown process. This implies similar inactivity for smaller and larger particles there (which are moved by wind less easily) and the plains ripples they compose. We conclude that plains ripples have not been active as recently as other bedforms described above. Individual plains ripples are oriented about  $\sim$ N26°E but are commonly grouped in echelon in alignments defining an older orientation of about N4°E. A clockwise change in wind direction is indicated from the older to the younger orientation of plains ripples, and then to the more recently active basalt sand ripples within Eagle (N38°E) and the Eagle crater bright wind streak (Fig. 3).

Ventifacts (erosional rock features formed by abrasion from wind-blown particles) provide a cumulative record of aeolian activity consistent with the changing wind patterns indicated by bedforms and albedo features. Small, elongate protrusions of light-toned rock occur adjacent to a subset of partially embedded, haematite-enriched

concretions. These features ('rock tails') are interpreted as erosional remnants in wind shadows behind the more resistant concretions (Fig. 2). Because these features occur in rock, they probably record an integrated, long-timescale history of the strongest, rarest wind events, and possibly the directions to major sediment sources. Concretion rock tail morphologies include raised ridges that taper in height and width away from concretions, as well as pedestals supporting concretions at their tips. Rock tails do not occur in every rock unit exposed at Eagle and Endurance craters. Orientations of rock tails show two lobes of formative winds: from  $284 \pm 28^\circ$  ( $n = 107$ ), and from  $135 \pm 25^\circ$  ( $n = 25$ ). The major lobe is aligned with winds from the west driving plains ripples (the N26°E and older N4°E orientations), and also includes some data consistent with the most recent strong winds from the northwest associated with the Eagle floor basaltic sand ripples and the bright wind streak. The second, minor lobe is consistent with winds from the southwest, which is the other recent wind direction associated with bright streaks in the landing ellipse.

A fundamental assumption is that the highest-energy wind events are the rarest, but can effect the most change. The preserved record is likely to reflect a biased series of progressively stronger and older but more obscure events, with even older or interleaved weaker events being unrepresented even if they were more typical. The most recent events at the landing site involve cycles of bright wind streak erasure and formation, caused by winds from approximately  $315^\circ$  or  $135^\circ$  exceeding  $u_{*t} \approx 2.0 \text{ ms}^{-1}$  (corresponding to a wind speed  $u$  of  $\sim 45 \text{ m s}^{-1}$  at 1 m above the bed) associated with large dust storms (Fig. 3). These wind events activate basaltic sand ripples in temporary particle traps like the floor of Eagle crater and, when strong enough, sweep accumulations of trapped material out on to the plains, supplying a sparse population of mobile sand grains that migrates from one trap to another. The armoured N26°E plains ripples have

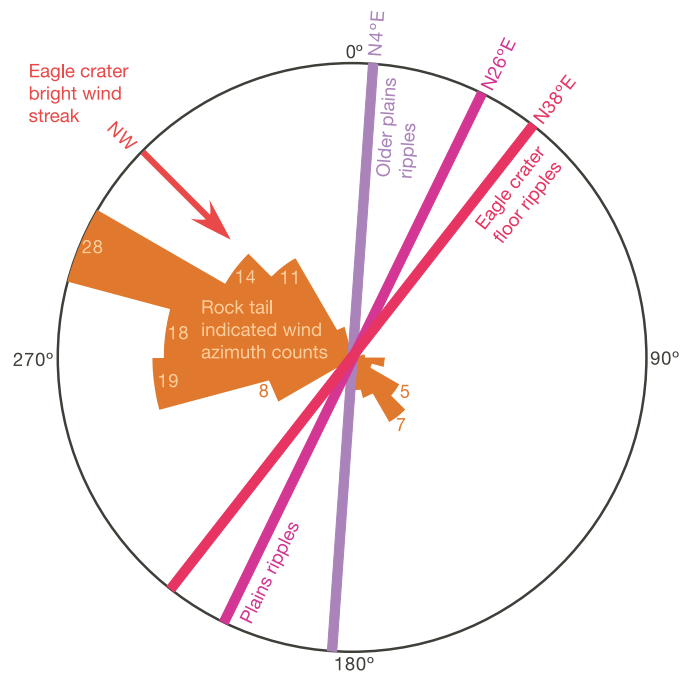


**Figure 3 | Orientations of rock tails, plains ripples, basaltic sand ripples on the floor of Eagle crater, and the Eagle crater bright wind streak.** Rock tail orientations (brown, with larger counts noted) span an azimuth range consistent with winds driving plains ripples (current and former orientations) in current N26°E and former N4°E orientations. Rock tails also seem to record erosion from winds consistent with the current wind streak direction and its opposite. A 40° clockwise rotation in major wind axes is indicated.

not been active as recently. These ripples formed when one or more strong wind events from around 296° partially reoriented a pre-existing set of plains bedforms. Winds during this process probably moved the 1–2-mm concretion fragments in creep only, driven by basaltic sand. Stronger winds capable of saltating the concretion fragments directly—exceeding  $u_* \approx 3.0 \text{ m s}^{-1}$  ( $u \approx 70 \text{ m s}^{-1}$  at 1 m)—probably would not have preserved any sign of the pre-existing N4°E bedform orientation.

However, excellent sorting of the 1–2-mm concretion fragment population currently armouring plains ripples indicates that very strong winds in the more distant past were capable of saltating these particles. These winds, with  $u_* > 3.0 \text{ m s}^{-1}$  ( $u > 70 \text{ m s}^{-1}$  at 1 m) may have been responsible for fragmenting a source supply of larger concretions through energetic collisions during transport, as well as sorting the fragments. It is unknown how the sorted population of concretion fragments armouring plains ripples became intermingled with the larger spherical concretions distributed across the flat areas between plains ripples. Winds capable of winnowing away finer grains but not coarser clasts can form deflational lags. As the surface concentration of larger, immobile clasts increases, the fraction of wind shear stress available to move loose, finer grains in between is reduced. Experiments with particle size frequencies broadly similar to inter-ripple areas at the landing site<sup>24,25</sup> suggest  $u_{*t}$  to move the finer grains will increase to speeds similar to those required to saltate the concretion fragments covering plains ripples. Thus deflation seems to have modified the plains to a uniform threshold shear velocity condition, with further deflation slowed by concretion fragment armour on the ripples, and larger, intact spherical concretions scattered across the flat areas between. The present-day inactivity of plains ripples indicates an upper bound for local  $u_*$  associated with current dust storms of  $\sim 3 \text{ m s}^{-1}$ , up to  $\sim 4 \text{ m s}^{-1}$  if the concretion fragments are pure haematite.

## METHODS

Calculations of  $u_{*t}$  use expressions derived from wind-tunnel experiments<sup>26,27</sup> and we specify the following conditions for all calculations except where noted: 250°K, 7 mbar CO<sub>2</sub>, martian gravity, and  $3.0 \text{ g cm}^{-3}$  particles. Wind speed,  $u$ , at height 1 m was estimated using an aerodynamic roughness of  $1 \times 10^{-4} \text{ m}$  in a standard logarithmic wind profile. This value of  $z_0$  is representative, used for comparative purposes only; for a given  $u_*$  or  $u_{*t}$  value, variations in  $z_0$  from  $5 \times 10^{-5} \text{ m}$  to  $5 \times 10^{-4} \text{ m}$  will raise or lower, respectively, all  $u$  estimates at  $z = 1 \text{ m}$  by 7–17%.

The lower bound of the regolith particle size range is uncertain because it is below the resolution (30 μm per pixel) of the Microscopic Imager<sup>28</sup>. This is especially relevant for regolith at the depth revealed by wheel trenching, which is cloddy and contains substantial fractions of grains unresolved by the Microscopic Imager. However, the fraction of basaltic grains <50 μm at the surface is likely to be small, because most grains on bulk surface deposits are resolved (2–5 pixels), as are individual dark grains silhouetted on light-toned outcrop<sup>23</sup>.

Received 23 November 2004; accepted 12 April 2005.

- Martin, L. J. & Zurek, R. W. An analysis of the history of dust activity on Mars. *J. Geophys. Res.* **98**, 3221–3246 (1993).
- Greeley, R., Lancaster, N., Lee, S. & Thomas, P. in *Mars* (eds Kieffer, H., Jakosky, B., Snyder, C. & Matthews, M. U.) 730–766 (Arizona Press, Tucson, 1992).
- Cantor, B. A., James, P. B., Caplinger, M. & Wolfe, M. J. Martian dust storms: 1999 Mars Orbiter Camera observations. *J. Geophys. Res.* **106**, 23653–23687 (2001).
- Veverka, J., Gierasch, P. & Thomas, P. Wind streaks on Mars: meteorological control of occurrence and mode of formation. *Icarus* **45**, 154–166 (1981).
- Thomas, P., Veverka, J., Gineris, D. & Wong, L. Dust streaks on Mars. *Icarus* **60**, 161–179 (1984).

- Sagan, C. *et al.* Variable features on Mars. 2. Mariner 9 global results. *J. Geophys. Res.* **78**, 4163–4196 (1973).
- Arvidson, R. E. Wind-blown streaks, splotches, and associated craters on Mars: Statistical analysis of Mariner 9 photographs. *Icarus* **21**, 12–27 (1974).
- Thomas, P. C., Veverka, J., Lee, S. & Bloom, A. Classification of wind streaks on Mars. *Icarus* **45**, 124–153 (1981).
- Greeley, R. & Thompson, S. D. Mars: Aeolian features and wind predictions at the Terra Meridiani and Isidis Planitia potential Mars Exploration Rover landing sites. *J. Geophys. Res.* **108**(E12), doi:10.1029/2003JE002110 (2003).
- Greeley, R. Wind tunnel simulations of light and dark streaks on Mars. *Science* **183**, 847–849 (1974).
- Bell, J. F. III, McCord, T. B. & Owensby, P. D. Observational evidence of crystalline iron oxides on Mars. *J. Geophys. Res.* **95**, 14447–14461 (1990).
- Klingelhöfer, G. *et al.* Jarosite and hematite at Meridiani Planum from Opportunity's Mössbauer spectrometer. *Science* **306**, 1740–1745 (2004).
- Rieder, R. *et al.* Chemistry of rocks and soils at Meridiani Planum from the Alpha Particle X-ray Spectrometer. *Science* **306**, 1746–1749 (2004).
- Yen, A. *et al.* An integrated view of the chemistry and mineralogy of martian soils. *Nature* doi:10.1038/nature03637 (this issue).
- Sagan, C. & Bagnold, R. A. Fluid transport on Earth and aeolian transport on Mars. *Icarus* **26**, 209–218 (1975).
- Iversen, J. D., Greeley, R. & Pollack, J. B. Windblown dust on Earth, Mars, and Venus. *J. Atmos. Sci.* **33**, 2425–2429 (1976).
- Greeley, R. & Iversen, J. D. *Wind as a Geological Process* 68–71 (Cambridge Univ. Press, Oxford, 1985).
- Tsoar, H. & Pye, K. Dust transport and the question of desert loess formation. *Sedimentology* **34**, 139–153 (1987).
- Edgett, K. S. & Christensen, P. R. The particle size of martian aeolian dunes. *J. Geophys. Res.* **96**, 22765–22776 (1991).
- Goossens, D. Aeolian dust ripples: Their occurrence, morphometrical characteristics, dynamics and origin. *Catena* **18**, 379–407 (1991).
- Greeley, R. *et al.* Rate of wind abrasion on Mars. *J. Geophys. Res.* **87**, 10009–10024 (1982).
- Arvidson, R. E. *et al.* Localization and physical properties experiments conducted by Opportunity at Meridiani Planum. *Science* **306**, 1730–1733 (2004).
- Soderblom, L. A. *et al.* Soils of Eagle Crater and Meridiani Planum at the Opportunity rover landing site. *Science* **306**, 1723–1726 (2004).
- Gillette, D. A. & Stockton, P. H. The effect of nonerodible particles on wind erosion of erodible surfaces. *J. Geophys. Res.* **94**, 12885–12893 (1989).
- Nickling, W. G. & McKenna Neuman, C. Development of deflation lag surfaces. *Sedimentology* **42**, 403–414 (1995).
- Iversen, J. D. & White, B. R. Saltation threshold on Earth, Mars and Venus. *Sedimentology* **29**, 111–119 (1982).
- White, B. R., Lacchia, B. M., Greeley, R. & Leach, R. N. Aeolian behaviour of dust in a simulated Martian environment. *J. Geophys. Res.* **102**, 25629–25640 (1997).
- Herkenhoff, K. *et al.* Evidence from Opportunity's Microscopic Imager for water on Meridiani Planum. *Science* **306**, 1727–1730 (2004).

**Acknowledgements** This work was performed for the Jet Propulsion Laboratory, California Institute of Technology, sponsored by the National Aeronautics and Space Administration. We are grateful for the efforts of the Mars Exploration Rover development and operations teams that made this work possible. We acknowledge the use of Mars Orbiter Camera images processed by Malin Space Science Systems that are available at [http://www.msss.com/moc\\_gallery/](http://www.msss.com/moc_gallery/).

**Authors Contributions** J.F.B. and W.C. provided Pancam and MiniTES analyses, respectively, of bright streak material. W.A.W. measured all rock tails. D.F. discovered the time dependence of wind streak orientations in MOC images. D.M. reviewed the APXS linear mixing work of R.S. R.S. also measured the ripple orientations, calculated  $u_{*t}$  and  $u$  values, worked out the aeolian history of the site, identified the discrepancy between particle size of basaltic ripples and  $u_F/u_{*t}$  ratio, and drafted the original and revised manuscripts. D.J. contributed key points relating to deflation at the site. R.S., D.J. and D.B. worked on potential explanations for the low  $u_F/u_{*t}$  ratio mobility of the basaltic sand. L.A.S. led the Science Operations Working Group during the bright streak rover operations. A.Y. advised on APXS calibration issues. All authors, particularly M.M., provided significant scientific guidance and/or editorial inputs.

**Author Information** Reprints and permissions information is available at [ngp.nature.com/reprintsandpermissions](http://ngp.nature.com/reprintsandpermissions). The authors declare no competing financial interests. Correspondence and requests for materials should be addressed to R.S. (rjs33@cornell.edu).